The Cryosphere Discuss., 9, 6791–6828, 2015
www.the-cryosphere-discuss.net/9/6791/2015/
doi:10.5194/tcd-9-6791-2015

The Cryosphere Discussions
Open Access
EGU

Greenland annual accumulation along the EGIG line, 1959–2004, from ASIRAS airborne radar and detailed neutron-probe density measurements

T. B. Overly[1], R. L. Hawley[1], V. Helm[3], E. M. Morris[2], and R. N. Chaudhary[1]

[1]Dartmouth College, Hanover, NH, USA
[2]Scott Polar Research Institute, Cambridge, UK
[3]Alfred Wegener Institute, Bremerhaven, Germany

Received: 1 September 2015 – Accepted: 3 November 2015 – Published: 14 December 2015

Correspondence to: T. B. Overly (thomas.b.overly@dartmouth.edu)

Published by Copernicus Publications on behalf of the European Geosciences Union.

Abstract

We report annual snow accumulation rates from 1959 to 2004 along a 250 km segment of the Expéditions Glaciologiques Internationales au Groenland (EGIG) line across central Greenland using Airborne SAR/Interferometric Radar Altimeter System (ASIRAS) radar layers and detailed neutron-probe (NP) density profiles. ASIRAS-NP accumulation rates are not statistically different (C.I. 95 %) from in situ EGIG accumulation measurements from 1985 to 2004. Below 3000 m elevation, ASIRAS-NP increases by 20 % for the period 1995 to 2004 compared to 1985 to 1994. Above 3000 m elevation, accumulation increases by 13 % for 1995–2004 compared to 1985–1994. Model snow accumulation results from the calibrated Fifth Generation Mesoscale Model modified for polar climates (Polar MM5) underestimate mean annual accumulation by 16 % compared to ASIRAS-NP from 1985 to 2004. We test radar-derived accumulation rates sensitivity to density using modelled density profiles in place of detailed NP data. ASIRAS radar layers combined with Herron and Langway (1980) model density profiles (ASIRAS-HL) produce accumulation rates within 3.5 % of ASIRAS-NP estimates. We suggest using Herron and Langway (1980) density profiles to calibrate radar layers detected in dry snow regions of ice sheets lacking detailed in situ density measurements, such as those observed by the IceBridge campaign.

1 Introduction

An understanding ice sheet mass balance requires knowledge of the gains and losses to the system. The IPCC conservatively estimates a 0.40 ± 0.15 m sea-level rise by the year 2100 (scenario RCP2.6 IPCC, 2014). Simplifications in assessing snow accumulation (the primary positive input to ice sheets) account for a portion of the uncertainty in potential sea-level rise. Ice cores provide records of past accumulation, while climate models reconstruct accumulation in regions lacking in situ measurements. Though detailed models such as the Fifth Generation Mesoscale

TCD
9, 6791–6828, 2015

Model modified for polar climates (Polar MM5) provide widespread spatial coverage of recent accumulation (1958–2007), the resulting accumulation rates primarily depend on interpolation between ground-truthed point locations. The simplification of accumulation rates from point-based measurements may be overcome using ice-penetrating radar. Ice penetrating radar reveals continuous isochronal layers within the dry-snow zone of ice sheets. Identifying the depth and age of these layers allows for the estimation of an accumulation rate. The depth of a given radar layer depends on the density of the snowpack through which the radar signal travels. Given this density and signal propagation relationship, the most accurate snow accumulation rates result from radar surveys collected simultaneously with in situ density measurements.

The European Space Agency's 2006 Airborne SAR/Interferometric Radar Altimeter System (ASIRAS) campaign detected annual accumulation layers along the Expéditions Glaciologiques Internationales au Groenland (EGIG) traverse across central Greenland (Hawley et al., 2006; de la Pena et al., 2010). Previous accumulation estimates using ASIRAS layers along EGIG incorporate a maximum of two density profiles to correct ASIRAS travel-time (and thus ASIRAS layer depth) (Hawley et al., 2006; de la Pena et al., 2010). Concurrent to the 2006 radar campaign, Morris and Wingham (2011) conducted detailed measurements of near-surface density using a neutron-probe (NP). Eight NP sites along a 250 km segment of the EGIG route provide ground-truthed density measurements for correcting ASIRAS travel-time through the ice sheet's surface (Fig. 1). We present annual accumulation rates from 1959 to 2004 derived from NP density adjusted ASIRAS layers (ASIRAS-NP accumulation record). We compare our ASIRAS-NP accumulation record to previous measurements of annual accumulation from shallow cores (Anklin and Stauffer, 1994; Fischer et al., 1995). Detailed density, collected in concert with an airborne radar survey, offers the opportunity to understand radar-derived accumulation rates' sensitivity to density. We test the ASIRAS accumulation rate's sensitivity to density using simple Herron and Langway modeled density profiles in place of detailed NP density measurements (ASIRAS-HL). Modeled density combined with radar layers may

TCD
9, 6791–6828, 2015

offer an alternative for deriving accumulation rates from radar layers lacking detailed ground-truthed density.

2 Background

2.1 EGIG line

Major joint European expeditions across central Greenland were conducted in 1958–1959 (EGIG1) and 1967–1968 (EGIG2). Shallow cores drilled along the route led to the first isotopic climate curves produced by Willi Dansgaard (Dansgaard, 2004). A 1990–1992 reconstruction of the EGIG line by Technische Universität Braunschweig led to glacio-meteorological, isotopic/chemical, and snow accumulation studies (Anklin and Stauffer, 1994; Fischer et al., 1995). These studies revealed around 0.45 m water equivalent accumulation per year (m w.e. a^{-1}) at the western portion of EGIG, decreasing to around 0.20 (m w.e. a^{-1}) along the eastern interior of the ice sheet. Fischer et al. (1995) found no long-term temporal changes in accumulation rates from 1955 to 1995.

Site T21 marks the approximate transition to the dry snow zone, with air temperatures upslope from T21 rarely exceeding 0 °C (Fig. 1) (Morris and Wingham, 2011). Morris and Wingham (2011) observed a transition in surface conditions approximately 10 km uphill from site T31. Down-slope from T31 katabatic winds compact the upper snow layer and form sastrugi. Elevations upslope from T31 experience less persistent winds, leaving a smooth surface with undisturbed summer surface hoar (Morris and Wingham, 2011).

Detailed analysis of snow accumulation builds upon previous accumulation studies using ice cores (Anklin and Stauffer, 1994; Bales et al., 2001, 2009; Banta and McConnell, 2007; McConnell et al., 2001), models (Box et al., 2004; Bromwich et al., 2001; Burgess et al., 2010; McConnell et al., 2000), and radar stratigraphy (Arcone

TCD
9, 6791–6828, 2015

et al., 2004, 2005; Eisen et al., 2008; Hawley et al., 2006; de la Pena et al., 2010; Spikes et al., 2004) to measure and model accumulation variability.

2.2 ASIRAS radar accumulation

The European Space Agency originally designed the Airborne Synthetic aperture Interferometric Radar Altimetry System (ASIRAS) to serve as a prototype for the CryoSat Mission (Stenseng et al., 2007). ASIRAS uses a Ku-band radar altimeter to measure ice sheet surface elevation and detect sub-surfaces layers. Stenseng et al. (2007) described the internal reflection horizons observed by ASIRAS as corresponding to density interfaces. ASIRAS radar has a carrier frequency of 13.5 GHz and instrument bandwidth $B = 1$ GHz. The radar transect discussed in this paper was collected using Low Altitude Mode (LAM). ASIRAS-LAM has 4096 echo samples, an uncompressed pulse length of $T_{uc} = 80\,\mu s$, an instrument sampling frequency of $F_s = 37.5$ MHz, resulting in a range bin resolution of $\Delta R = 0.109$ m, using the range-resolution equation from (Cullen, 2010):

$$\Delta R = \frac{T_{uc} F_s c}{2BN_s} \quad (1)$$

where c is the speed of light, $\sim 299\,792\,458\,m\,s^{-1}$.

Hawley et al. (2006) measured eight annual accumulations (1995–2002) at site T21 using ASIRAS radar. The study used a single NP density profile, T21, to calculate radar travel-time through snowpack and depth to the sub-surface layers. Hawley et al. (2006) establish ASIRAS internal reflection horizons as annual accumulation layers, correlating high density winter peaks with local peaks in radar power return. ASIRAS accumulation layers, examined down to 10 m depth, produced a mean annual accumulation of $0.47\,m\,w.e.\,a^{-1}$ (similar to Anklin and Stauffer, 1994; Fischer et al., 1995). Hawley et al. (2006) found decreasing accumulation with increasing elevation and short-scale variability in line with Fischer et al. (1995) and Box et al. (2004).

TCD
9, 6791–6828, 2015

Hawley et al. (2006) observe upward curved reflectors in areas of steep slope and accumulation-driven layering, in agreement with Black and Budd (1964).

de la Pena et al. (2010) presented mean accumulation rates for the period 1998–2003, calculated from six ASIRAS internal reflection horizons along 200 km of the EGIG route. de la Pena et al. (2010) used Hawley et al. (2006)'s published T21 neutron-probe density values and a Summit density profile (located 150 km north of the EGIG line) to linearly interpolate density values, calculate radar travel-time, estimate layer depth, and compute accumulation rates along the EGIG route. de la Pena et al. (2010) report an average accumulation of 0.36 m w.e. a^{-1} with high spatial and temporal variability, and a clear decreasing accumulation gradient from west to east along the EGIG line. The observed accumulation gradient is consistent with previous studies of Anklin and Stauffer (1994), Fischer et al. (1995), Burgess et al. (2010), and the interannual variability observed by Fischer et al. (1995). de la Pena et al. (2010) presented a 15–20 % increase in accumulation above 3000 m over the past 20–25 yrs compared to Anklin and Stauffer (1994).

Both the de la Pena et al. (2010), Hawley et al. (2006)'s studies rely on a maximum of two density profiles to constrain radar travel-time for determination of layer depth. We expand the range of ground-truthed density measurements using eight neutron-probe density measurements along the EGIG line.

2.3 EGIG-Ground in situ measurements

2.3.1 Shallow core accumulation

Anklin and Stauffer (1994) drilled eleven shallow firn cores (e.g. T21, referred to as T-sites), 8 to 10 m depth, about every 50 km along the EGIG line. Using hydrogen peroxide (H_2O_2) analysis and snow density to identify the seasonal signal, Anklin and Stauffer (1994) report annual accumulation from 1969 to 1989 for T-sites along the EGIG line. Anklin and Stauffer (1994) found accumulation rates that fit with the general understanding of water vapor transport and snow accumulation across the Greenland

TCD
9, 6791–6828, 2015

Ice Sheet: higher accumulations along the coast gradually decreasing with increasing elevation. Accumulation rates of 0.44 m w.e. a^{-1} along the western portion of the EGIG line decrease to 0.25 m w.e. a^{-1} at the eastern margin. Anklin and Stauffer (1994) found large variations of local annual accumulation rates from 1979 to 1989, with typical standard deviations of 10 to 25 %. Changes in annual accumulation correlated from site to site. Temporally, annual accumulation increased slightly in central Greenland and decreased slightly at middle and low elevations.

Fischer et al. (1995) drilled eighteen shallow firn cores along the EGIG line during field campaigns in 1990 and 1992. Annual accumulation rates from 1984–1989 were determined by counting seasonally varying tracers $\delta^{18}O$ and major ions. Measurements were collected at approximately eight samples per year. The 1990 campaign used seasonally varying hydrogen peroxide (H_2O_2) analysis (in collaboration with Anklin and Stauffer, 1994) to determine summer maxima of flourimetric profiles. Fischer et al. (1995) observed distinct winter/summer pairings in the upper snow. Fischer et al. (1995) found layer thickness and accumulations similar to Anklin and Stauffer (1994), with highest along the western portion of EGIG (0.47 to 0.43 m w.e. a^{-1}), decreasing to the east (0.25 to 0.20 m w.e. a^{-1}, though fewer measurements exist to support the eastern accumulation rates). Fischer et al. (1995) argue for accumulation variation as large scale phenomenon based on distinct valleys and ridges along EGIG. The short timespan of the study, 1984 to 1989, limited the identifiable temporal trend (Fischer et al., 1995).

2.3.2 Neutron-probe densities and accumulation

Morris and Wingham (2011) collected near-surface in situ neutron-probe (NP) density measurements along a 365 km section of the EGIG line in the Spring and Autumn of 2004 and Spring and Summer of 2006 (Morris and Wingham, 2014). The 2006 traverse coincided with airborne observations of sub-surface layers using the Airborne SAR/Interferometric Radar Altimeter System (ASIRAS). The probe used by Morris and Wingham (2011) consists of an annular radioactive americium-241/beryllium source

TCD
9, 6791–6828, 2015

of fast neutrons around a cylindrical detector of slow (thermal) neutrons (Morris and Cooper, 2003). The fast neutrons lose energy by scattering as they move through the snow. The count rate of slow neutrons arriving back at the detector per unit time relates to the density of the snow (Morris and Wingham, 2011). Morris (2008) derived theoretical calibration equations for count rate and snow density. Descriptions of the neutron-probe data collection can be found in Morris and Wingham (2011), Morris and Wingham (2014).

The Morris and Wingham (2011) traverses span ice-sheet elevations of 1940 to 3201 m, with accumulation generally decreasing with increasing elevation. Morris and Wingham (2011) collected seventeen "T-site" NP density profiles and accumulation rates (eight NP T-sites of this study mapped on Fig. 1). The neutron-probe measured snow density from the surface down to approximately 13 m depth at the T-sites along the EGIG traverse. Density fluctuates between high-density winter peaks and low-density summer troughs (see Morris and Wingham, 2011). The vertical distance between successive winter density peaks defines a NP annual layer (Hawley et al., 2008). Morris and Wingham (2011) observe that the density peaks lie in winter snow and are formed during the following summer when warm temperatures promote densification in the near surface layers. This transition in snow density marks the annual seasonal change detected by ASIRAS (Hawley et al., 2006; de la Pena et al., 2010). The snow thickness between density peaks, adjusted to mean water-equivalent using density measurements, provides an estimate of annual accumulation (Hawley et al., 2008; Morris and Wingham, 2011).

3 Methods

3.1 ASIRAS traced layers

We focus on a 250 km segment of the EGIG line spanning eight NP T-sites (Fig. 1). We trace 48 layers down to 20 m depth from a 29 April 2006 ASIRAS flight radargram

TCD
9, 6791–6828, 2015

(Fig. 2). Our radar profile starts with 0 km distance at the site of T21a at 2700 m elevation and ends 250 km to the east just beyond the ice divide below 3200 m. The radargram has been processed from SAR processed level_1b ASIRAS data using the following signal processing techniques: waveform alignment, stacking, and gain. Each column of the radargram represents the centered mean of the surrounding 100 columns (hence 100 columns "stacked" into one record, representing approximately three horizontal meters). The ASIRAS signal weakens with increasing depth through the snowpack, thus we apply a ramped gain to the signal to enhance the visual contrast of the radargram. The ramped gain resembles an exponential gain, resulting in a 3× enhancement of layer intensity at 15 m depth and an 8× enhancement at 20 m depth. Deeper layers appear faint near the western portion of EGIG (0 to 75 km) where seasonal melt in the upper layers attenuates the radar signal.

We trace layers by tracking the maximum reflected power. The trace progresses by searching the adjacent column for a maximum power reflected within the vertical range of a moving window. Automated layer tracing occurs one layer at a time with visual inspection and user approval of the final traced layer. The shallowest (1st) layer represents the 2005 accumulation surface and the deepest (48th) traced layer represents the 1959 accumulation year (Autumn 1958 to Autumn 1959) (Fig. A1). The deeper layers fade in intensity along the western section of the line (0–75 km) and also with increasing depth along the rest of the line (75–250 km). The exact depth depends on the ASIRAS electromagnetic wave speed v ($\mathrm{m\,s^{-1}}$) through the snowpack. Electromagnetic wave speed v relates to the real part of the dielectric permittivity ϵ_r (dimensionless) which in the near-surface can be related to density ρ ($\mathrm{kg\,m^{-3}}$) by (Kovacs et al., 1995):

$$v = \frac{c}{\sqrt{\epsilon_r}} \tag{2}$$

$$\epsilon_r = (1 + 8.45 \times 10^{-4}\rho)^2 \tag{3}$$

where c is the speed of light in a vacuum ($\sim 3 \times 10^8\ \mathrm{m\,s^{-1}}$).

TCD
9, 6791–6828, 2015

Signal travel-time will change based on the density of the snowpack. The travel-time, measured in nanoseconds, corresponds to a given depth (or distance traveled by the ASIRAS signal pulse) in the snowpack. For example, dense coastal snowpack slows the signal speed compared to a less dense interior snowpack. Near the coast 45 ns of travel-time equals 5.10 m depth while the same travel-time in the interior would equal 5.15 m depth. ASIRAS corrected with a coastal density profile gives a depth of 20.03 m at 190 ns. The same 190 ns travel-time reaches 20.24 m depth using the interior NP profile.

Both ASIRAS-NP and ASIRAS-HL accumulation rates have the same radar-time layer positions. The density used to adjust the radar signal propagation determines the depth and thickness of an annual accumulation layer. ASIRAS-NP, discussed in Sect. 3.3.1, interpolates densities between eight NP density profiles (Sect. 3.2) to adjust layer depths. ASIRAS-HL, discussed in Sect. 3.2.2, uses ASIRAS layers adjusted with HL density profiles to calculate layer depths and thicknesses.

3.2 Density profiles

3.2.1 Neutron-probe density

Detailed density profiles allow for more accurate calculations of ASIRAS radar, travel-time through the snowpack. Morris and Wingham (2011) made repeat NP density measurements at the T-sites in the Spring and Autumn of 2004 and 2006. We combine the 2004 and 2006 measurements, extending ground-truthed centimeter resolution density measurements to 11 m depth. We use 16 previously published (Morris and Wingham, 2011) density profiles from eight T-sites (T21a, T23, T27, T31, T35, T39, T41) in the dry-snow zone above 2700 m (Fig. 2). The deepest NP measurements are 11 m, while our deepest ASIRAS layer reaches 30 m depth. We estimate densities below 11 m depth using the centimeter resolution density 50 m GISP2 B-core (NSIDC, 1997) at Summit. The eastern edge of EGIG experiences the same climate conditions as Summit. The easternmost NP density measurement (T41)

TCD
9, 6791–6828, 2015

at 10 m depth (0.538 g m^{-3}) is similar to the GISP2 B-core density value at 10 m core depth (0.529 g m^{-3}). We use GISP2 B-core "Shifted" densities to correct radar travel-time from the deepest NP measurement to the deepest ASIRAS layer. The western edge of EGIG, at 2700 m elevation, has a 10 m density of 0.559 g m^{-3}. We assume the rate of densification below 10 m depth is similar at T21a, T41, and GISP2. We shift the GISP2 profile at 10 m depth to start where T21a NP density profile ends.

3.2.2 Herron and Langway model density

The logistical challenge of ice-sheet wide density surveys limits the number of detailed density measurements. A limited number of NP logging systems exist, and transport and deployment of an active radionucleid source complicates matters further. Herron and Langway (1980)'s simple empirical model of polar snow densification provides an alternative for estimating ice sheet density in the absence of in situ density. The model allows us to generate a density profile at any point along EGIG with three input parameters: mean annual accumulation A, mean annual temperature T, and initial surface snow density ρ_i. The model has two stages of densification for depths above and below the "critical density" $\rho = 0.55\,\mathrm{Mg\,m^{-3}}$. The model equations used for density ρ at depth h for the two stages of densification:

Pre-critical:

$$\rho_h = \frac{\rho_i \zeta_0}{1+\zeta_0}$$

$$\zeta_0 = \exp\left[\rho_i k_0 h + \ln\left(\frac{\rho_0}{\rho_i - \rho_0}\right)\right]$$

$$k_0 = 11 \cdot \exp\left(\frac{-10\,160}{R \cdot T}\right)$$

Post-critical:

$$\rho_h = \frac{\rho_i \zeta_1}{1+\zeta_1}$$

$$\zeta_1 = \exp\left[\rho_i k_1 \frac{(h - h_{0.55})}{A^{0.5}} + \ln\left(\frac{0.55}{\rho_i - 0.55}\right)\right]$$

$$k_1 = 575 \cdot \exp\left(\frac{-21\,400}{R \cdot T}\right)$$

TCD
9, 6791–6828, 2015

where $h_{0.55} = \frac{1}{\rho_i k_0}[\ln \frac{0.55}{\rho_i - 0.55} - \frac{\rho_0}{\rho_i - \rho_0}]$ and gas constant $R = 8.314\,\mathrm{J\,K^{-1}\,mol^{-1}}$. We calculate densities along EGIG using mean annual accumulation from Burgess et al. (2010), temperatures from Steffen and Box (2001), and Morris and Wingham (2011)'s T-site surface densities as inputs to Herron and Langway (1980)'s model. We use densities generated from Herron and Langway (1980)'s model to adjust radar travel-time and derive the ASIRAS-HL accumulation rate as a comparison to the NP derived ASIRAS-NP accumulation rates.

3.3 Accumulation rates from ASIRAS

3.3.1 ASIRAS-NP: accumulation rate using neutron-probe densities

The sixteen NP density profiles at eight T-sites (T21a, T23, T27, T31, T35, T39, T41) bound by the combined T21a and GISP2 b-core densities on the west and the T41 and GISP2 b-core on the east, provide the anchor points for interpolating depth-density values at every point along the EGIG line. We calculate annual accumulation rates from 1959 to 2004 at the T-sites (Table A1). We refrain from calculating a 2005 annual accumulation due to its proximity to the surface. The NP based densities represent the most detailed density measurements along EGIG and correct ASIRAS travel-time through the snowpack to create the ASIRAS-NP accumulation rates.

3.3.2 ASIRAS-HL: accumulation rate using herron and langway densities

Taking detailed NP density measurements remains beyond the scope of most radar surveys. We explore using simple Herron and Langway (1980) model densities (HL) to produce accumulation rates from ASIRAS radar layers (ASIRAS-HL). We examine the accumulation rate difference when using modeled density data (ASIRAS-HL) and using detailed density (ASIRAS-NP). Using spatially continuous input parameters of accumulation, temperature, and surface density, we generate HL density profiles for 74 038 locations along the 250 km segment of EGIG.

TCD
9, 6791–6828, 2015

We examine accumulation rate sensitivity to density by reducing the number of HL density profiles used to correct layer depth along the 250 km EGIG segment. Distance intervals and their corresponding number of density profiles per the 250 km EGIG segment are: 250 km (HL250, 1 profile), 125 km (HL125, 2 profiles), 50 km (HL50, 5 profiles), 30 km (HL30, 8 profiles), and 15 km (HL15, 17 profiles). We interpolate between the HL profiles to obtain a density profile at every point along EGIG.

3.4 EGIG-Ground accumulation measurements

We combine shallow firn core records from Anklin and Stauffer (1994) and NP based accumulation rates calculated by Morris and Wingham (2011) to establish EGIG-Ground records spanning 1978–2004 at T21, T27, T31, T41. Site T43 has twelve annual accumulations from 1976 to 1988 but no NP measurements (Anklin and Stauffer, 1994). Anklin and Stauffer (1994) cores generally span 1978 to 1988 while the Morris and Wingham (2011) accumulation rates span the mid-1980's to 2004. We use the mean of the two records at site T41 where the two records overlap. Sites T21, T27, and T31 do not have overlapping records, with no accumulation rates for years 1989 and 1990 at T21 and T27 and 1989 for T31. These EGIG-Ground records serve as a basis for comparison of accumulation rates derived from ASIRAS layers (Fig. 3).

4 Results

4.1 ASIRAS-NP accumulation rate

The layers detected by ASIRAS and adjusted with the detailed NP profiles provide a spatially continuous record of accumulation across 250 km of the EGIG route. We trace layers to thirty meters depth and report accumulation rates for forty-six layers spanning 1959–2004 (Fig. A1). The mean accumulation rate for the entire 250 km EGIG segment is 0.337 m w.e. a^{-1} from 1959 to 2004. We focus our reported results on the period 1985 to 2004, during which EGIG-Ground measurements exist for

TCD
9, 6791–6828, 2015

comparison. Figure 2 displays spatial and temporal variations in layers across the EGIG segment.

Temporally, accumulation rates increase over time, with the onset of increase occurring in the mid-1970s. From 1959 to 1964, mean accumulation was 0.277 m w.e. a^{-1}. From 1965 to 1974, mean accumulation was 0.270 m w.e. a^{-1}. From 1975 to 1984, mean accumulation was 0.327 m w.e. a^{-1}. Mean ASIRAS-NP accumulation from 1985 to 1994 was 0.329 m w.e. a^{-1}. Accumulation for the period 1995 to 2004 (0.382 m w.e. a^{-1}) increases by 16 % compared to the previous 10 year period. Table 1 summarizes the 10 year mean accumulation results. Please see the Table A1 for detailed accumulations from 1959 to 1984.

Spatially, accumulation decreases with increasing elevation and distance from the coast. Mean annual accumulation for 1985 to 2004 at T21a (0 km) is 0.462 m w.e. a^{-1}, gradually decreasing to 0.380 m w.e. a^{-1} at T31, 0.297 m w.e. a^{-1} at T41, and 0.254 m w.e. a^{-1} at the 250 km mark (Table A1). Using the transition in surface conditions occurring near T31 to divide EGIG, we examine accumulation rate changes over time above and below T31. Below T31, mean accumulation increased by 20 % over the 10 year period 1995 to 2004 (0.465 m w.e. a^{-1}) compared to the 1985 to 1994 period (0.387 m w.e. a^{-1}). Above T31, with undisturbed summer surface hoar from less persistent winds, accumulation increased by 13 % over the 10 year period 1995 to 2004 (0.335 m a^{-1}) compared to the 1985 to 1994 period (0.296 m a^{-1}). In the following sections we validate ASIRAS-NP accumulation rates by comparison to EGIG-Ground point accumulation records (Anklin and Stauffer, 1994; Morris and Wingham, 2011) and spatially continuous Polar MM5 accumulation rates (Burgess et al., 2010).

4.2 ASIRAS-NP vs. EGIG-Ground

The published EGIG-Ground in situ accumulation records discussed in Sect. 3.4 serve as the "known" accumulation rate to which we compare our ASIRAS-NP record. We focus on four sites (T21, T27, T31, T41) that have accumulation records from both Anklin and Stauffer (1994) and Morris and Wingham (2011). We also include

TCD
9, 6791–6828, 2015

the T43 (Crete) record, which has twelve measurements from 1976 to 1988 (Anklin and Stauffer, 1994). Figure 3 presents these comparisons at the five T-sites. "Box and whisker" plots of accumulation values for EGIG-Ground, ASIRAS, and Polar MM5 appear in the lower panel of Fig. 3. We compare the full records year by year using a nonparametric Wilcoxon sign-rank test designed for two populations with paired observations. The test is performed on the difference of paired yearly accumulations. The ASIRAS-NP and EGIG-Ground accumulation differences have distributions whose medians are zero at sites T21, T27, T31, and T41. The zero median of the paired and differenced records indicate the ASIRAS-NP and EGIG-Ground accumulations come from identical populations. The paired records at sites T21, T27, T31, T41, though identical, have varying strengths of similarity. Table A2 presents the probability, p, of observing a test statistic as or more extreme than the observed value. The Wilcoxon signed-rank test at site T43, with only twelve ground measurements for comparison, shows EGIG-Ground and ASIRAS-NP are significantly different. In addition to the year by year comparisons, we found that 1985 to 2004 EGIG-Ground and ASIRAS-NP accumulation rates are not statistically different at sites T21, T27, T31, T41 from Anklin and Stauffer (1994) and Morris and Wingham (2011) (Table 2). We conducted an analysis of variance test to compare means of the 20 year (1985–2004) annual snow accumulation for ASIRAS-NP and EGIG-Ground, and the Polar MM5 and ASIRAS-NP accumulation for 1978 to 2004. Significance differences were determined for alpha < 0.05. Again, EGIG-Ground and ASIRAS accumulation at site T43 are significantly different. Comparing the yearly accumulations for the entire record, Pearson's correlation coefficients for EGIG-Ground and ASIRAS accumulations range from 0.75 to 0.16 (Table A3).

4.3 ASIRAS-NP vs. Polar MM5

ASIRAS-NP and Polar MM5 accumulation rates from 1978 to 2004 positively correlate at T-sites T21, T23, T27, T41, T43 (Table A3). An ANOVA comparison of means for 1978 to 2004 between Polar MM5 and ASIRAS-NP shows mean accumulations are

TCD
9, 6791–6828, 2015

statistically different at T-sites T21, T27, T31, and T41. Polar MM5 and ASIRAS-NP accumulations at T43 are not statistically different. Using a Wilcoxon signed-rank test year to year comparisons show significant statistical differences between Polar MM5 and ASIRAS-NP at T-sites T21, T27, T31, T41. The mean comparison excludes site T43, which lacks NP measurements. Polar MM5 mean accumulations along EGIG are significantly lower for the time period coincident with EGIG-Ground measurements, 1985 to 2004 (Fig. 4). We focus on the period 1985 to 2004 to calculate standard uncertainty ($\frac{\sigma}{\sqrt{n}}$, where σ = standard deviation and $n = 20$).

Mean Polar MM5 accumulation (0.293 m w.e. a^{-1}) from 1985 to 2004 across the entire 250 km EGIG segment is 17 % lower than ASIRAS-NP (0.355 m w.e. a^{-1}). Mean ASIRAS-NP and Polar MM5 accumulations rates from 1985 to 2004 differ spatially along EGIG. Using the transition in surface conditions occurring near T31 to divide EGIG, Polar MM5 underestimates accumulation by 28 % downslope from T31 compared to ASIRAS-NP. Above T31, with undisturbed summer surface hoar from less persistent winds, mean Polar MM5 accumulation is 20 % lower than ASIRAS-NP. Accumulation rates change over time with differing rates above and below T31. ASIRAS-NP accumulations from 1995 to 2005 are 35 % higher than Polar MM5 accumulations down-slope of T31. Below T31 from 1985 to 1994 ASIRAS-NP accumulations are 21 % higher than Polar MM5. East of T31, where surface conditions stabilize, ASIRAS-NP accumulation is 23 % higher for 1985–1994 and 16 % higher for 1995–2004, relative to Polar MM5.

4.4 ASIRAS-NP vs. ASIRAS-HL: accumulation rate sensitivity to density

Mean percentage accumulation differences between ASIRAS-NP and ASIRAS-HL decrease with increasing age/depth of the layers (Fig. 5). Figure 5 plots the mean difference between ASIRAS-NP and ASIRAS-HL for the upper five (2000–2004), lower five (1985–1989), and 1985–2004 layers. On average the deeper the layer, the lower the difference between ASIRAS-NP and ASIRAS-HL accumulation rates. The upper

TCD
9, 6791–6828, 2015

five layers differ by 4 % on average. The lower five layers differ by 3.2 %. Overall, for the period 1985–2004, mean ASIRAS-HL accumulation is 4.5 % lower than ASIRAS-NP accumulation.

We test sensitivity to density by limiting the number of HL density profiles along EGIG and interpolating density values between the profiles. Using one density profile (HL250 km) for the entire 250 km EGIG segment results in a 10 % difference in ASIRAS-NP and ASIRAS-HL. Incorporating two density profiles (HL125 km) halves the accumulation difference from 10 to 5 %. The ASIRAS-NP and ASIRAS-HL accumulation difference reduces to 3 % for HL50 km (5 profiles), HL30 km (8 profiles), and HL15 km (17 profiles).

5 Discussion

5.1 ASIRAS-NP accumulation rate

The ASIRAS layers combined with NP density data improve understanding of accumulation between T-sites, showing detailed peaks and valleys in accumulation as seen and attributed to topography by Arcone et al. (2005), Hawley et al. (2006), Black and Budd (1964), Miége and et. al. (2013). The undulating layers observed in Fig. 2 reinforce ice core observations of high spatial variability (Spikes et al., 2004). Spatial variability decreases with increasing depth, as layers undergo compaction. The fluctuations of layer depth and vertically aligned dips and peaks may indicate surface accumulation anomalies (Arcone et al., 2005). A gradual horizontal migration of undulations over time could produce spatially periodic accumulation rates, as described by Arcone et al. (2005). Undulations preserved from year to year are visible east of T27 at 60 km and from 125 to 175 km along the EGIG line (Fig. 2 and Fig. A1). The oscillations are visible in the long term mean temporal accumulation rate in Fig. 4. Visual inspection of layer thickness for a given year (Fig. 2 and Fig. A1) allows us to argue for high confidence in the extreme values measured by ASIRAS-NP.

TCD
9, 6791–6828, 2015

In comparison to historical records, de la Pena et al. (2010) and Hawley et al. (2014) observed accumulation increases of 19 and 10 % over the last 30 and 52 years, respectively, in high-elevation interior Greenland. We report a 16 % increase in accumulation for the period 1995–2004 compared to 1985–1994. We observe an east-west gradient of increasing accumulation, with lower accumulation increases in the east and higher increases to the west. The east-west gradient strengthens from 1995 to 2004, when ASIRAS-NP is 20 % higher than ASIRAS-NP below T31 and 13 % higher above T31.

5.2 ASIRAS-NP vs. EGIG-Ground

The patterns observed by Anklin and Stauffer (1994), Fischer et al. (1995), Morris and Wingham (2011) at the T-sites align with the overall trend observed by de la Pena et al. (2010) along EGIG of decreasing accumulation from the coast to the interior. The year-to-year comparisons from Fig. 3 using Paired Wilcoxon signed-rank span every year with observations for both ASIRAS-NP and EGIG-Ground. Year to year comparisons show that ASIRAS-NP tracks the EGIG-Ground measurements consistently. EGIG-Ground accumulation minima and maxima are not always consistent across the EGIG route for a given year (e.g. the T31 record's maxima occurs in 1995, while T27 and T41 records have near minimum values for 1995). Fluctuation from site to site in the EGIG-Ground record is due to the limited spatially extent of a given shallow core or snowpit. Accumulation extremes seen in the ASIRAS-NP record are consistent across the T-sites (low in 1998, high in 1996). A Wilcoxon signed-rank test at site T43 shows EGIG-Ground and ASIRAS are significantly different, yet the Pearson's correlation coefficient at T43 are strongly positive. These results may be due to the small number of EGIG-Ground measurements (twelve) at T43.

TCD
9, 6791–6828, 2015

5.3 ASIRAS-NP vs. Polar MM5

Polar MM5 underestimates accumulation relative to ASIRAS-NP and EGIG-Ground (Fig. 4). Mean Polar MM5 accumulation from 1985 to 2004 along EGIG is 0.06 m (17 %) lower than ASIRAS-NP measurements. The mean 0.06 m difference falls within Polar MM5's standard deviation of accumulation along EGIG (0.025–0.075) (Burgess et al., 2010). The consistent underestimate of Polar MM5 accumulation relative to ASIRAS-NP and EGIG-Ground may be explained by the measurements used to tune Polar MM5. Burgess et al. (2010) added spatial and temporal resolution to Greenland ice sheet accumulation by calibrating the Polar MM5 using firn cores and meteorological stations data. Burgess et al. (2010) re-sample the Polar MM5's 24 km horizontal grid output to a 1.25 km equal-area grid using bilinear interpolation (Burgess et al., 2010; Rignot et al., 2008). The 24 km original spacing results in approximately eight Polar MM5 data points along the 250 km EGIG line. These eight Polar MM5 points were tuned from a network of cores and automatic weather stations and thus were not forced to correspond exactly with cores along EGIG. Burgess et al. (2010) omit the majority of the T-site accumulation rates along EGIG, including only sites T31, T41, and T43. ASIRAS-NP provides detailed accumulation measurements every 3 m, nearly continuous tracking along EGIG relative to Polar MM5. The increased detail may contribute to the majority of the difference in accumulation rates.

Yearly comparisons of the entire record of ASIRAS-NP and Polar MM5 snow accumulations (Fig. 3) show positive correlations for T21a, T23, T27, T41, T43 (Table A3). Correlations between ASIRAS-NP and Polar MM5 demonstrate the model's utility for predicting the relative year-to-year accumulation trend. ASIRAS-NP and Polar MM5 both track the general accumulation trend of higher accumulation near the coast decreasing to lower interior accumulation rates as elevation increases (Fig. 4). The observed accumulation gradient experiences a noticeable change in surface conditions near site T31 (Morris and Wingham, 2011). Down-slope from T31 katabatic winds pack the upper snow layer and form sastrugi, which may influence spatial

TCD
9, 6791–6828, 2015

variability and preservation of accumulation layers. Signal preserved in the upper ASIRAS-NP accumulation layers would be absent in the Polar MM5 record, possibly explaining Polar MM5's 28 % accumulation underestimate compared to ASIRAS-NP below T31. Elevations upslope from T31 experience less persistent winds, leaving a smooth surface with undisturbed summer surface hoar, with a mean Polar MM5 accumulation 24 % lower than ASIRAS-NP. The spatial gradient has a noticeable temporal component when comparing ASIRAS-NP and Polar MM5. From 1985 to 1994, ASIRAS-NP accumulation is 28 % higher than Polar MM5 on both sides of T31. The east-west gradient strengthens from 1995 to 2004, when ASIRAS-NP is 24 % higher than Polar MM5 below T31 and 16 % higher above T31. Polar MM5's recent accumulation rates near EGIG rely on firn cores drilled prior to 1995 and limited automatic weather stations at high elevation. Thus recent observed increases in accumulation at high elevation due to increased moisture availability from warming (de la Pena et al., 2010; Hawley et al., 2014) may not appear in the Polar MM5 record.

5.4 ASIRAS-NP vs. ASIRAS-HL: accumulation rate sensitivity to density

Subtracting the ASIRAS-HL and ASIRAS-NP accumulation rates tests the radar-derived accumulation rate's sensitivity to density. The ASIRAS layers' position in radar time remains constant between the ASIRAS-NP and ASIRAS-HL. Density, which determines radar velocity and therefore water-equivalent depth, is the lone variable between ASIRAS-NP and ASIRAS-HL accumulation records. As expected, the largest differences in accumulation occur where NP and HL densities differ most. Accumulation differences reduce as HL densities approach NP densities. NP density profiles provide detailed vertical resolution of seasonal density fluctuation. Seasonal density fluctuations are most prominent in the near surface layers and in areas with large variability in temperature and accumulation (e.g. coastal, lower elevations). Though the simple three parameter Herron and Langway (1980) model cannot capture the detailed seasonal density variations, the model's general trend in the near-surface generates ASIRAS-HL accumulation rates within 4.5 % of ASIRAS-NP. NP and HL

TCD
9, 6791–6828, 2015

densities resemble each other most at deeper depths as compaction smooths seasonal fluctuations in density. Thus the deeper layers have the smallest mean percentage accumulation difference (3 %) (Fig. 5). The low (4.5 %) mean accumulation differences along EGIG indicate that modeled density values provide reasonable accumulation estimates in areas with low variability in density and where detailed density profiles are unavailable. Differences in accumulation decrease with increasing depth/age of the layers, as the HL model densities approach NP densities. Below 11 m depth, differences are related to Summit GISP2b-Shifted and Summit GISP2b shallow density core bounding the west (0 km) and east (250 km) margins, respectively, of the EGIG line. No dominant spatial pattern of accumulation differences emerges from west to east. The mean of the lower five accumulation years (1985–1989) account for the smallest accumulation differences from 60 to 250 km. The largest differences along EGIG occur on the eastern slope (225–250 km) where ASIRAS-NP is constrained by a Summit density core, and thus the largest difference in ASIRAS-NP and ASIRAS-HL densities. Abrupt jumps in mean percent accumulation difference occur where the number of layers included in the average change.

Recall the spatially continuous nature of the density inputs for the ASIRAS-HL accumulation record (74 038 unique HL density profiles spaced 3 m apart). These density inputs were driven by highly resolved HL model inputs of accumulation, temperature and surface density. ASIRAS-HL accumulation accuracy relative to ASIRAS-NP may be due to these model inputs. We test this possibility with the HL250 km, HL125 km, etc., accumulation records, which rely on a limited number of density profiles and interpolation. The moderate reduction from 7 to 4.5 % accumulation difference for HL250 km and HL125 km is likely due to the linear gradients (increasing accumulation downslope, decreasing elevation, increasing temperature) of the HL model input parameters along the 250 km EGIG segment. The two density profiles of HL125 km cover both the lower and upper range of the gradients. The interpolation between these two contain the majority of density variation seen in the ASIRAS-NP, thus accounting for the 4 % mean accumulation difference between ASIRAS-HL125 km

TCD
9, 6791–6828, 2015

and ASIRAS-NP. An average 3.2 % percent accumulation difference can be obtained using 5 HL profiles at 50 km spacing. This finding stands to improve accuracy for radar-derived accumulation rates and serve as a guideline for correcting the wealth of IceBridge radar data.

6 Conclusions

Point-based measurements such as ice cores and weather stations provide the basis for current accumulation estimates. Models and interpolation between these points provide spatially continuous estimates of accumulation. Radar-detected annual accumulation layers offer a physical observation connecting point-based measurements. Detailed NP density measurements provide accurate radar travel-time velocities and exact densities for water-equivalent conversion, improving accuracy of annual accumulation rates from ASIRAS. We report spatially continuous annual accumulation rates from 1959 to 2004 along a 250 km segment of EGIG. Our ASIRAS-NP rates are not statistically different from EGIG-Ground point measurements spanning 1985–2004. Mean ASIRAS-NP accumulation along EGIG is 23 % higher than the mean Polar MM5 model estimate. An east to west accumulation gradient strengthens from 1995–2004, when ASIRAS-NP is 35 % higher than Polar MM5 downslope from T31 and 23 % higher upslope from T31. The ASIRAS-NP observed increases in mean accumulation may relate to increased warming and availability of moisture at higher elevations.

The similarity between ASIRAS and EGIG-Ground demonstrates that the ASIRAS layers, adjusted with NP density, produce accurate estimates of accumulation along a continuous 250 km segment of the EGIG line. We recognize the challenge of obtaining detailed density measurements and demonstrate the use of simple HL models to derive adequate accumulation estimates. Using Herron and Langway (1980) profiles at 50 km intervals produces ASIRAS-HL accumulation rates within 3 % of ASIRAS-NP estimates. Using similar methods, radar layers detected in dry

TCD
9, 6791–6828, 2015

snow regions of ice sheets, such as those observed by the IceBridge campaign, calibrated with a minimal number of Herron and Langway (1980) density profiles, may produce accumulation rates within the uncertainty of accumulation best-estimates using detailed density profiles.

Acknowledgements. This work was supported by the European Space Agency (ESA) as a part of the CryoSat program and by National Aeronautics and Space Administration (NASA) Grants NNX10AP04G and NNX10AG22G. We thank all team members involved in the CryoVex 2006 campaign. We are especially grateful to the in situ calibration and validation team for their efforts collecting detailed neutron-probe data. We thank the reviewers and editor Marco Tedesco for their comments and handling of the manuscript.

References

Anklin, M. and Stauffer, B.: Pattern of annual snow accumulation along a west Greenland flow lone: no significant change observed during recent decades, Tellus B, 46, 294–303, 1994. 6793, 6794, 6795, 6796, 6797, 6803, 6804, 6805, 6808, 6823, 6825, 6826

Arcone, S., Spikes, V., Hamilton, G., and Mayewski, P. A.: Stratigraphic continuity in 400 MHz short-pulse radar profiles of firn in West Antarctica, Ann. Glaciol., 39, 195–200, 2004. 6794

Arcone, S., Spikes, V., and Hamilton, G.: Stratigraphic variation within polar firn caused by differential accumulation and ice flow: interpretation of a 400 MHz short-pulse radar profile from West Antarctica, J. Glaciol., 51, 407–422, 2005. 6795, 6807

Bales, R. C., McConnell, J. R., Mosley-Thompson, E., and Csatho, B.: Accumulation over the Greenland ice sheet from historical and recent records, J. Geophys. Res.-Atmos., 106, 33813–33825, 2001. 6794

Bales, R. C., Guo, Q., Shen, D., McConnell, J., Du, G., Burkhart, J. F., Spikes, V., Hanna, E., and Cappelen, J.: Annual accumulation for Greenland updated using ice core data developed during 2000–2006 and analysis of daily coastal meteorological data, J. Geophys. Res., 114, D06116, doi:10.1029/2008JD011208, 2009. 6794

Banta, J. and McConnell, J. R.: Annual accumulation over recent centuries at four sites in central Greenland, J. Geophys. Res., 112, D10114, doi:10.1029/2006JD007887, 2007. 6794

TCD
9, 6791–6828, 2015

Black, H. and Budd, W.: Accumulation in the region of Wilkes, Wilkes Land, Antarctica, J. Glaciol., 5, 3–15, 1964. 6796, 6807, 6824

Box, J. E., Bromwich, D. H., and Bai, L. S.: Greenland ice sheet surface mass balance 1991–2000: application of Polar MM5 mesoscale model and in situ data, J. Geophys. Res., 109, D16105, doi:10.1029/2003JD004451, 2004. 6794, 6795

Bromwich, D. H., Chen, Q. S., Bai, L. S., Cassano, E., and Li, Y.: Modeled precipitation variability over the Greenland ice sheet, J. Geophys. Res., 106, 33891–33908, 2001. 6794

Burgess, E., Forster, R. R., Box, J. E., Mosley-Thompson, E., Bromwich, D. H., Bales, R. C., and Smith, L.: A spatially calibrated model of annual accumulation rate on the Greenland Ice Sheet (1958–2007), J. Geophys. Res., 115, F02004, doi:10.1029/2009JF001293, 2010. 6794, 6796, 6802, 6804, 6809, 6825, 6826

Cullen, R.: CryoVEx Airborne Data Products Description, ASIRAS 2.6.1, European Space Agency, ESTEC, Noordwijk, Netherlands, 2010. 6795

Dansgaard, W.: Frozen Annals: Greenland Ice Sheet Research, Aage V. Jenkins Fonde (Denmark), 1st Edn., available at: http://www.nbi.ku.dk/english/www/willi/dansgaard/tilbage-til-groenland/, last access: 12 August 2015, 2004. 6794

de la Peña, S., Nienow, P., Shepherd, A., Helm, V., Mair, D., Hanna, E., Huybrechts, P., Guo, Q., Cullen, R., and Wingham, D.: Spatially extensive estimates of annual accumulation in the dry snow zone of the Greenland Ice Sheet determined from radar altimetry, The Cryosphere, 4, 467–474, doi:10.5194/tc-4-467-2010, 2010. 6793, 6795, 6796, 6798, 6808, 6810

Eisen, O., Frezzotti, M., Genthon, C., Isaksson, E., Magand, O., van den Broeke, M. R., Dixon, D., Ekaykin, A., Holmlund, P., Kameda, T., Karlöf, L., Kaspari, S., Lipenkov, V., Oerter, H., Takahashi, S., and Vaughan, D. G.: Ground-based measurements of spatial and temporal variability of snow accumulation in East Antarctica, Rev. Geophys., 46, RG2001, doi:10.1029/2006RG000218,2008. 6795

Fischer, H., Wagenbach, D., Laternser, M., and Haeberli, W.: Glaciometerological and isotopic studies along the EGIG line, central Greenland ice sheet, J. Glaciol., 41, 515–527, 1995. 6793, 6794, 6795, 6796, 6797, 6808

Hawley, R. L., Morris, E. M., Cullen, R., Nixdorf, U., Shepherd, A. P., and Wingham, D. J.: ASIRAS airborne radar resolves internal annual layers in the dry-snow zone of Greenland, Geophys. Res. Lett., 33, L04502, doi:10.1029/2005GL025147, 2006. 6793, 6795, 6796, 6798, 6807

TCD
9, 6791–6828, 2015

Hawley, R. L., Morris, E. M., and McConnell, J.: Intruments and methods rapid techniques for determining annual accumulation applied at Summit, Greenland, J. Glaciol., 54, 839–845, 2008. 6798

Hawley, R. L., Courville, Z., Kehrl, L., Lutz, E., Osterberg, E., Overly, T., and Wong, G.: Recent accumulation variability in northwest Greenland from ground-penetrating radar and shallow cores along the Greenland Inland Traverse, J. Glaciol., 60, 375–382, 2014. 6808, 6810

Herron, M. and Langway Jr., C.: Firn densification: an empirical model, J. Glaciol., 25, 373–385, 1980. 6792, 6801, 6802, 6810, 6812, 6813

IPCC: Climate Change 2014 Synthesis Report, edited by: Pachauri, K., Meyer, L., and core writing team, Intergovernmental Panel on Climate Change, IPCC Secretariat, Geneva, Switzerland, 2014. 6792

Kovacs, A., Gow, A. J., and Morey, R. M.: The in-situ dielectric constant of polar firn revisted, Cold Reg. Sci. Technol., 23, 245–256, 1995. 6799

McConnell, J. R., Mosley-Thompson, E., Bromwich, D. H., Bales, R. C., and Kyne, J. D.: Interannual variations of snow accumulation on the Greenland Ice Sheet (1985-1996): new observations versus model predictions, J. Geophys. Res.-Atmos., 105, 4039–4046, 2000. 6794

McConnell, J. R., Lamorey, G., Hanna, E., Mosley-Thompson, E., Bales, R. C., Belle-Oudry, D., and Kyne, J. D.: Annual net snow accumulation over southern Greenland from 1975 to 1998, J. Geophys. Res., 106, 33827–33837, 2001. 6794

Miége, C., Forster, R. R., Box, J. E., Burgess, E. W., McConnell, J. R., Pasteris, D. R., and Spikes, V. B.: Southeast Greenland high accumulation rates derived from firn cores and ground-penetrating radar, Ann. Glaciol., 54, 322–332, 2013. 6807

Morris, E. M.: A theoretical analysis of the neutron-scattering method for measuring snow and ice density, J. Geophys. Res., 113, F03019, doi:10.1029/2007JF000962, 2008. 6798

Morris, E. M. and Cooper, J.: Density measurements in ice boreholes using neutron scattering, J. Glaciol., 49, 599–604, 2003. 6798

Morris, E. M. and Wingham, D. J.: The effect of fluctuations in surface density, accumulation and compaction on elevation change rates along the EGIG line, central Greenland, J. Glaciol., 57, 416–430, 2011. 6793, 6794, 6797, 6798, 6800, 6802, 6803, 6804, 6805, 6808, 6809, 6823, 6824, 6825, 6826

Morris, E. M. and Wingham, D. J.: Densification of polar snow: measurements, modeling, and implications for altimetry, J. Geophys. Res.-Earth, 119, 349–365, 2014. 6797, 6798

TCD
9, 6791–6828, 2015

NSIDC: GISP2 B-Core Density. The Greenland Summit Ice Cores CD-ROM, Tech. rep., National Snow and Ice Data Center, University of Colorado, Boulder, 1997. 6800

Rignot, E., Box, J., and Burgess, E.: Mass balance of the Greenland ice sheet from 1958 to 2007, Geophys. Res. Lett., 35, L20502, doi:10.1029/2008GL035417, 2008. 6809

Spikes, V., Hamilton, G., Arcone, S., Kaspari, S., and Mayewski, P.: Variability in accumulation rates from GRP profiling on the West Antarctic plateau, Ann. Glaciol., 39, 238–244, 2004. 6795, 6807

Steffen, K. and Box, J.: Surface climatology of the Greenland ice sheet: Greenland Climate Network 1995–1999, J. Geophys. Res., 106, 33951–33964, 2001. 6802

Stenseng, L., Hvidegaard, S., Skourup, H., Forsberg, R., Andersen, C., Hanson, S., Cullen, R., and Helm, V.: Airborne Lidar and Radar Measurements In and Around Greenland CryoVEx 2006, Tech. rep., Danish National Space Institute, Copenhagen, Denmark, 2007. 6795

TCD
9, 6791–6828, 2015

Table 1. Summary table of Mean Accumulation Rates, 1985–2004, for Fig. 4. Percentage change relative to previous 10-year period.

Period	Accum	Percent change
1959–2004	0.337 ± 0.03	–
1995–2004	0.382 ± 0.03	16 %
1984–1995	0.328 ± 0.02	0 %
1975–1984	0.327 ± 0.01	21 %
1965–1974	0.270 ± 0.01	−3 %
1959–1964	0.277 ± 0.01	–

TCD
9, 6791–6828, 2015

Table 2. Summary table of Mean Accumulation Rates, 1985–2004, for Fig. 4.

Study	T21	T27	T31	T41
EGIG-Ground*	0.488 ± 0.03	0.405 ± 0.02	0.385 ± 0.02	0.294 ± 0.01
ASIRAS	0.455 ± 0.02	0.409 ± 0.02	0.378 ± 0.01	0.297 ± 0.01
MM5	0.370 ± 0.01	0.333 ± 0.01	0.311 ± 0.005	0.257 ± 0.005

TCD
9, 6791–6828, 2015

Table A1. Mean annual accumulation (m w.e.) at T-sites along EGIG.

Year	T21	T21a	T23	T27	T31	T35	T39	T41	T43
Lat	70.54	70.59	70.62	70.78	70.91	70.98	71.04	71.08	71.12
Lon	−43.03	−42.79	−42.58	−41.54	−40.64	−39.55	−38.46	−37.92	−37.32
2004	0.64	0.67	0.64	0.56	0.49	0.40	0.36	0.33	0.31
2003	0.56	0.58	0.61	0.48	0.43	0.37	0.33	0.30	0.31
2002	0.39	0.41	0.39	0.38	0.38	0.34	0.30	0.32	0.35
2001	0.56	0.58	0.48	0.41	0.36	0.36	0.32	0.29	0.28
2000	0.56	0.54	0.52	0.42	0.35	0.28	0.29	0.25	0.23
1999	0.49	0.41	0.52	0.54	0.47	0.46	0.39	0.38	0.37
1998	0.40	0.42	0.40	0.31	0.31	0.25	0.23	0.24	0.21
1997	0.45	0.44	0.46	0.42	0.39	0.33	0.31	0.29	0.26
1996	0.50	0.51	0.50	0.46	0.47	0.47	0.44	0.39	0.41
1995	0.61	0.55	0.59	0.53	0.43	0.41	0.34	0.33	0.30
1994	0.34	0.32	0.35	0.34	0.32	0.26	0.26	0.25	0.21
1993	0.36	0.36	0.34	0.28	0.27	0.23	0.23	0.23	0.25
1992	0.29	0.33	0.32	0.30	0.29	0.29	0.29	0.26	0.26
1991	0.58	0.53	0.50	0.40	0.39	0.39	0.34	0.35	0.33
1990	0.44	0.46	0.49	0.46	0.42	0.39	0.36	0.34	0.33
1989	0.40	0.40	0.41	0.40	0.38	0.30	0.30	0.28	0.27
1988	0.40	0.40	0.41	0.34	0.30	0.26	0.27	0.24	0.24
1987	0.39	0.39	0.38	0.33	0.34	0.33	0.28	0.28	0.26
1986	–	–	0.33	0.43	0.40	0.34	0.32	0.34	0.30
1985	–	–	0.66	0.49	0.44	0.43	0.31	0.26	0.25
1984	–	–	0.47	0.42	0.32	0.26	0.27	0.27	0.28
1983	–	–	0.47	0.51	0.48	0.35	0.34	0.35	0.31
1982	–	–	0.32	0.29	0.27	0.27	0.28	0.25	0.28
1981	–	–	0.41	0.33	0.29	0.27	0.21	0.22	0.20
1980	–	–	0.27	0.38	0.33	0.29	0.29	0.26	0.24
1979	–	–	0.32	0.23	0.29	0.26	0.28	0.26	0.28

TCD
9, 6791–6828, 2015

Table A1. Continued.

Year	T21	T21a	T23	T27	T31	T35	T39	T41	T43
Lat	70.54	70.59	70.62	70.78	70.91	70.98	71.04	71.08	71.12
Lon	−43.03	−42.79	−42.58	−41.54	−40.64	−39.55	−38.46	−37.92	−37.32
1978	–	–	0.46	0.43	0.35	0.34	0.28	0.28	0.24
1977	–	–	0.57	0.51	0.38	0.35	0.34	0.27	0.28
1976	–	–	0.40	0.39	0.38	0.37	0.28	0.31	0.24
1975	–	–	0.42	0.54	0.42	0.27	0.30	0.31	0.34
1974	–	–	0.31	0.30	0.43	0.37	0.34	0.28	0.25
1973	–	–	0.33	0.31	0.29	0.26	0.24	0.23	0.26
1972	–	–	–	–	0.32	0.33	0.28	0.31	0.31
1971	–	–	–	–	0.32	0.31	0.26	0.25	0.25
1970	–	–	–	–	0.28	0.28	0.28	0.27	0.25
1969	–	–	–	–	0.41	0.32	0.23	0.24	0.22
1968	–	–	–	–	0.30	0.28	0.28	0.26	0.25
1967	–	–	–	–	0.29	0.28	0.28	0.28	0.26
1966	–	–	–	–	0.27	0.31	0.22	0.23	0.19
1965	–	–	–	–	0.24	0.22	0.23	0.22	0.23
1964	–	–	–	–	0.34	0.35	0.34	0.34	0.28
1963	–	–	–	–	0.31	0.31	0.29	0.29	0.29
1962	–	–	–	–	0.24	0.24	0.20	0.23	0.23
1961	–	–	–	–	0.23	0.24	0.24	0.25	0.23
1960	–	–	–	–	0.28	0.28	0.27	0.27	0.24
1959	–	–	–	–	0.34	0.35	0.32	0.33	0.30

TCD
9, 6791–6828, 2015

Table A2. Paired Wilcoxon Rank Sum comparison of Accumulation Fig. 3. The Wilcoxon signed rank test is a nonparametric test for two populations when the observations are paired. *p* is the probability of observing a test statistic as or more extreme than the observed value under the null hypothesis. Alternate hypothesis states that the data in ***x*** come from a continuous distribution with median different than 0. Tests the null hypothesis that data in the vector ***x*** come from a distribution whose median is zero at the 5 % significance level.

Paired	T21	T27	T31	T41	T43
			p		
EGIG-Ground and ASIRAS	0.98 (17)	0.89 (19)	0.92 (24)	0.19 (27)	0.34 (12)
EGIG-Ground and Polar MM5	0.01 (20)	0.001 (23)	0.003 (25)	0.01 (27)	0.83 (11)

TCD
9, 6791–6828, 2015

Table A3. Pearson's Correlation Coefficients for Accumulation Fig. 3. EGIG-Ground vs. ASIRAS and EGIG-Ground vs. Polar MM5.

Paired	T21	T27	T31	T41	T43
			Pearson's *R*		
EGIG-Ground and ASIRAS-NP	0.46 (16)	0.19 (21)	0.21 (24)	0.42 (27)	0.56 (13)
EGIG-Ground and Polar MM5	−0.04 (22)	0.32 (21)	0.15 (24)	0.35 (27)	0.21 (11)
ASIRAS-NP and Polar MM5	0.56 (18)	0.45 (27)	0.43 (27)	0.53 (27)	0.46 (27)

TCD
9, 6791–6828, 2015

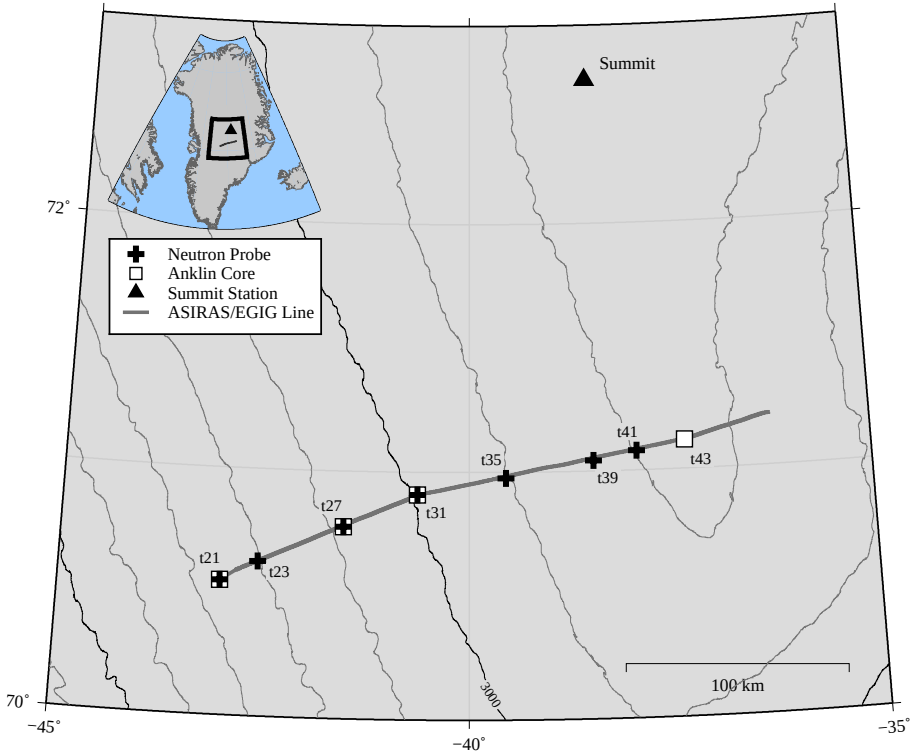

Figure 1. Field locations along a portion of the Expédition Glaciologique Internationale au Groenland (EGIG) traverse. The 250 km segment of ASIRAS radar data discussed in this paper spans 2600 to 3200 m elevation. Black crosses ✚ show neutron-probe density T-sites from Morris and Wingham (2011). White squares □ show Anklin and Stauffer (1994) shallow cores. The filled triangle ▲ shows the location of Summit Station for reference. 100 m contour intervals above 2000 m elevation are displayed. Scale bar accurate at 71° N latitude.

TCD
9, 6791–6828, 2015

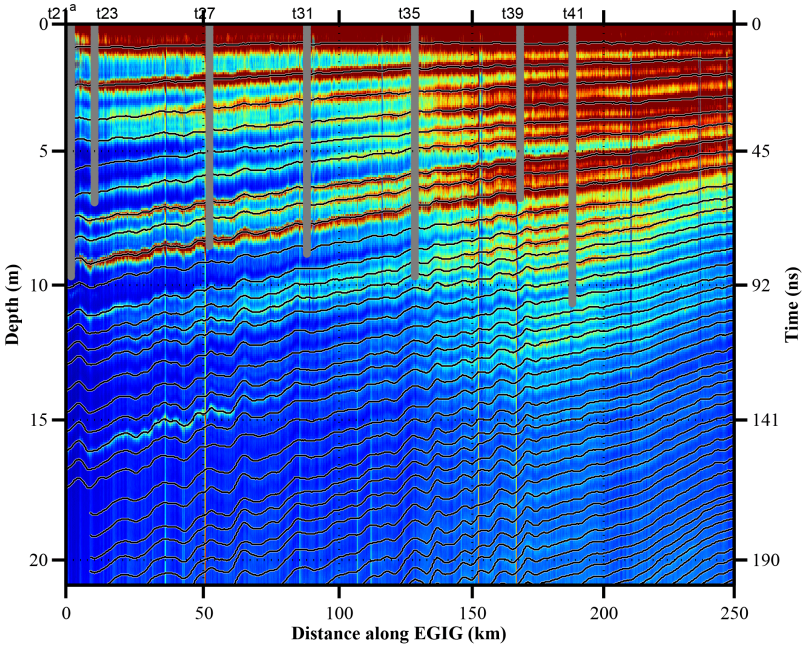

Figure 2. ASIRAS radargram of a portion of the forty-seven traced internal reflection horizons (IRHs), or layers, down to 20 m depth. The uppermost layer represents the 2005 accumulation year. Distance along EGIG corresponds with gray line in Fig. 1, with 0 km starting at 2700 m on the western slope and 250 km ending below 3200 m on the eastern slope of the Greenland Ice Sheet. Near-surface layers appear vivid down to 10 m depth. The left axis shows depth for NP and IRHs. The right axis shows two-way travel time of an ASIRAS radar pulse. High coastal accumulation rates, evident from thicker western layers from 0 to 50 km, gradually thin with increasing elevation and orographic deposition of accumulation approaching the ice divide at 210 m distance. Topographic effects related to local surface features (described by Black and Budd, 1964) may explain layer undulations. Vertical gray lines indicate the position and depth of Morris and Wingham (2011) NP density measurements.

TCD
9, 6791–6828, 2015

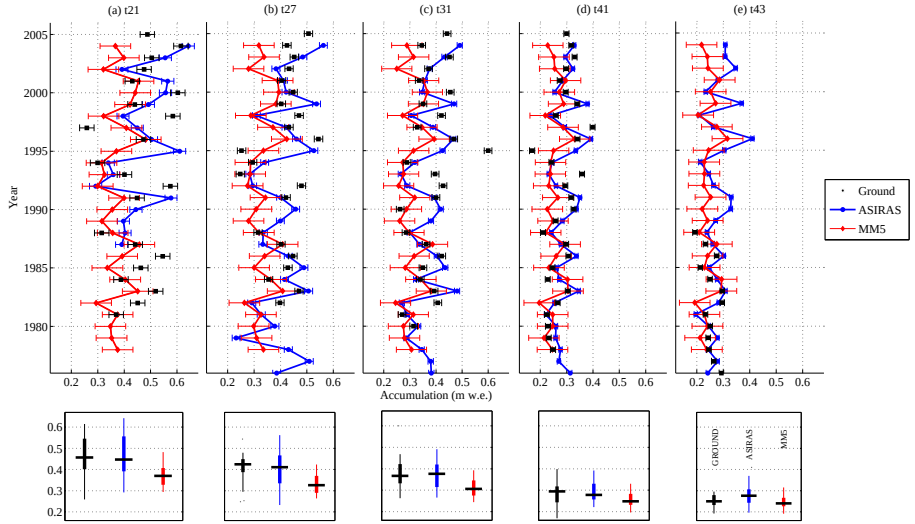

Figure 3. Mean annual accumulation rates at T21, T27, T31, T41, and T43, from ASIRAS-NP, Polar MM5 Model (Burgess et al., 2010), and combined EGIG-Ground measurements from Anklin and Stauffer (1994) and Morris and Wingham (2011). ASIRAS-NP and EGIG-Ground accumulation rates from 1985 to 2004 are not statistically different at sites T21, T27, T31, and T41. Polar MM5 accumulations are generally lower than ASIRAS accumulations but mostly remain within each other's uncertainty. Accumulation rate and fluctuation of accumulation decreases from T21 to T43 as site elevation increases and accumulation rates stabilize across the interior of the ice sheet. The general agreement of the three accumulation rates demonstrates ASIRAS's ability to track accumulation across the EGIG route. The lower panels display the mean accum rates. The EGIG-Ground mean is significantly different from Polar MM5 means at T21, T27, T31 for the entire record.

TCD
9, 6791–6828, 2015

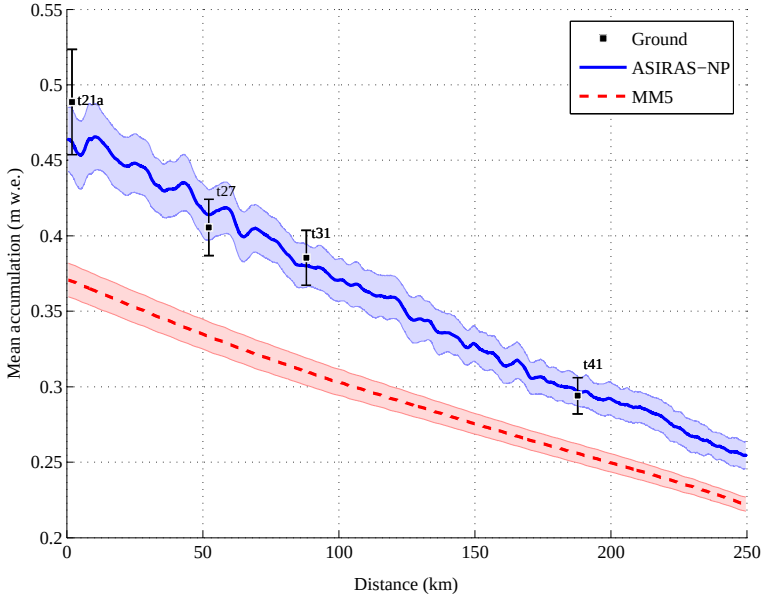

Figure 4. Mean water-equivalent accumulations rates from 1985 to 2004 along EGIG line. Solid dark blue line shows this study's accumulation derived from ASIRAS layers and NP densities. Dashed red line shows Burgess et al. (2010)'s Polar MM5 modeled snow accumulation. Black squares depict mean accumulation from T-sites with NP/Core EGIG-Ground measurements from Anklin and Stauffer (1994) and Morris and Wingham (2011) spanning 1985–2004 (T21, T27, T31, T41). These mean accumulation rates summarize the annual rates presented in Fig. 3. Compared to the annual accumulation rates in Fig. 3, averaging over 1985 to 2004 reveals Polar MM5's underestimate of accumulation compared to ASIRAS-NP and EGIG-Ground in situ estimates. Radar-derived accumulation rates are highest near the coast where density values have the largest range. Standard uncertainties displayed are for accumulation values from 1985 to 2004.

TCD
9, 6791–6828, 2015

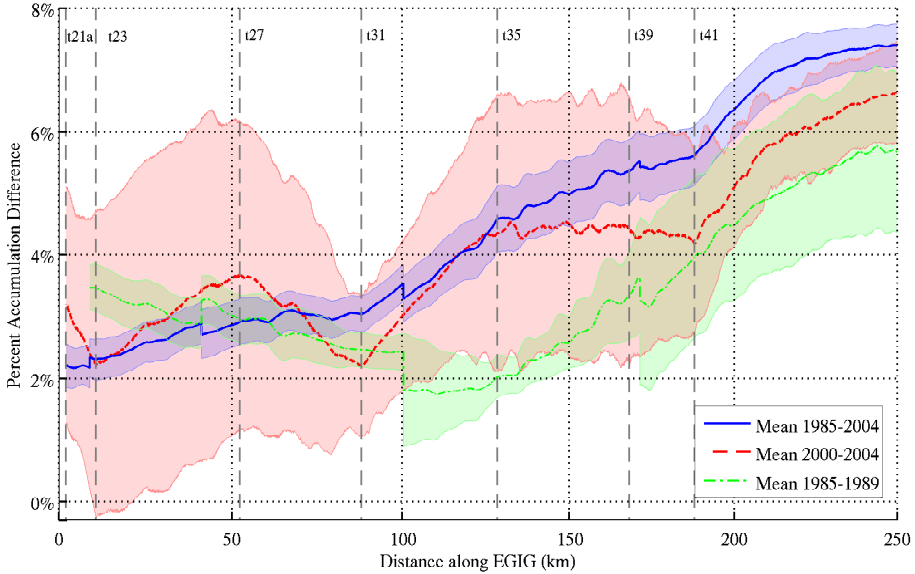

Figure 5. Mean percentage accumulation difference between ASIRAS-NP and ASIRAS-HL for the upper five (2000–2004), lower five (1985–1989), and 1985–2004 layers. In general, differences in accumulation decrease with increasing depth/age of the layers. ASIRAS-HL accumulation differs from ASIRAS-NP accumulation by 4.5 % for the 1985–2004 period. The low mean differences across the 250 km EGIG segment indicate that modeled densities provide accurate accumulation estimates in radar survey regions lacking in situ density measurements.

TCD
9, 6791–6828, 2015

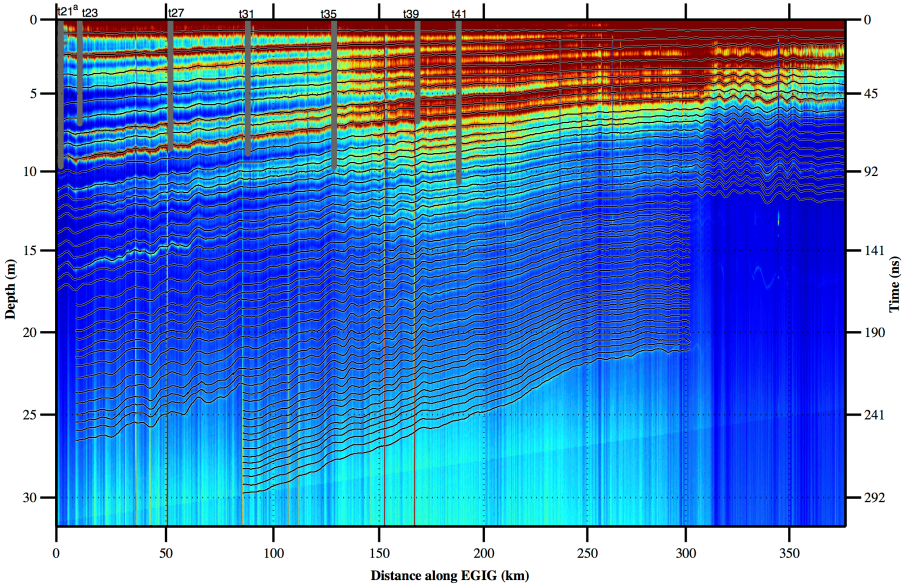

Figure A1. ASIRAS radargram of the forty-seven traced internal reflection horizons (IRHs), or layers, down to 30 m depth. The uppermost layer represents the 2005 accumulation year. The deepest layer represent 1959. Distance along EGIG corresponds with T21 in Fig. 1, with 0 km starting at 2700 m on the western slope and extending beyond 350 km where layer visibility decreases on the eastern slope of the Greenland Ice Sheet.

TCD
9, 6791–6828, 2015